TD-05-057
December 21, 2005

Electromagnetic Instabilities in Nb_3Sn RRP Strands and Cables

E. Barzi, G. Ambrosio, L. Del Frate, V.V. Kashikhin, D. Turrioni,
R. Yamada, A.V. Zlobin

Abstract— Results of studies of electromagnetic instabilities in Nb_3Sn strands and cables produced using the Restack Rod Process technology are presented. The critical current of the strands was measured using the voltage-current and voltage-field methods. Magnetization was measured using a balanced coil magnetometer. Effects of strand deformation were studied. A superconducting current transformer with a maximum DC current of 28 kA was used for cable testing at self-fields under various experimental conditions. These results are in good agreement with magnet test data as well as with experimental studies of similar strands and cables. The strand and cable parameters, equipment and measurement methods used, and the results of the measurements are herein described.

I. INTRODUCTION

After attaining success in a 10 T dipole mirror made of 1 mm Powder-in-Tube (PIT) Nb_3Sn strands with an effective filament diameter of ~50 μm, and replicating this success with two subsequent reproducible 10 T PIT dipoles [1, 2], the next step in FNAL R&D in high field accelerator magnets was to increase the dipole field by using larger J_c superconductors. However, as the instability problem became more relevant [3], and it was experimentally shown [4, 5] that an effective filament diameter, d_{eff}, of excessive size reduces the I_c at low field to ≤20% of its expected value, the dipoles were redesigned to accommodate a cable made of 0.7 mm strands. A 0.7 mm 54/61 filament design made with the Restack Rod Process (RRP) by Oxford Superconducting Technology (OST) was chosen to fabricate cable. Two dipole mirrors, HFDM04 and HFDM05 [2], were fabricated and tested. They reached only ~50% of the expected short sample limit. This note presents RRP strand and cable data, including those from the witness samples reacted with the coils, and discuss the effect of conductor parameters on the observed magnet performance.

II. STRANDS AND CABLES DESCRIPTION

Three different multifilamentary RRP strands produced by OST were used for this study. The strand cross-sections are shown in Fig. 1 and strand parameters are summarized in Table I, using also data from [6]. The 54/61 filament strand was also used to fabricate 38 and 39-strand Rutherford cables ID's 891 and 892, and rectangular cable 911R at LBNL. This latter cable was then keystoned at FNAL. The 108/127 filament strands were used to fabricate 27-strand cables HFDA-RC and HFDA-KS at FNAL. The cables description is in Table II. Cable 891-D was used for FNAL mirror magnet

HDFM04 and cable 911 for dipole model HFDM05. Cable HFDA-KS is used to fabricate a single layer small racetrack.

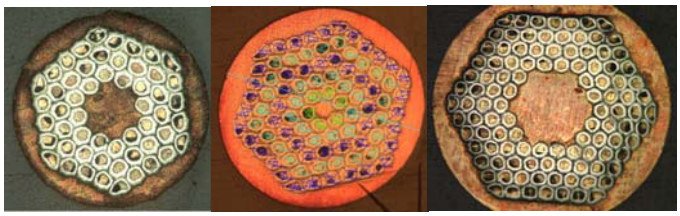

Fig. 1. 54/61 (left), 90/91 (center) and 108/127 filament (right) RRP designs.

TABLE I
STRANDS DESCRIPTION

Billet ID	7054-60	8079	8195-97
Technology	RRP	RRP	RRP
No. of filaments	54/61	90/91	108/127
Strand diameter, mm	0.7	0.7	1.0 0.7
I_c(12 T), A	~520	~500	~900 ~450
D_{eff}, μm	85	72	84
Geometric filament size, μm	61-75	52-65	64-75
RRR	40	300	300 200
Twist pitch, mm	12	-	25
Cu fr., %	50	41	49

TABLE II
CABLES DESCRIPTION

Cable ID	892-A	892-B	892-C	892-D	891-A	891-C	891-D	911	HFDA-RC	HFDA-KS
Billet ID	7054-60	7054-60	7054-60	7054-60	7054-60	7054-60	7054-60	7054-60	8197-97	8197-97
No. of strands	39	39	38	38	39	39	39	39	27	27
Strand diameter, mm	0.7	0.7	0.7	0.7	0.7	0.7	0.7	0.7	1.0	1.0
Cable cross-section	Rect.	Rect.	Rect.	Rect.	Keyst.	Keyst.	Keyst.	Keyst.	Rect.	Keyst.
Packing factor, %	88.5	90	88.5	88	85	88.5	90	87.2	81	86

To expand the range of d_{eff} in strands and to compare strand and cable measurements, some strands were rolled down (before reaction) as shown in Fig. 2 to various sizes. Fig. 2 also shows the two orientations of rolled strand samples with respect to the external magnetic field that were used to test I_c and I_s. The so-called short edge configuration, where the longest size of the strand is perpendicular to the field, is shown at left, and the long edge at right.

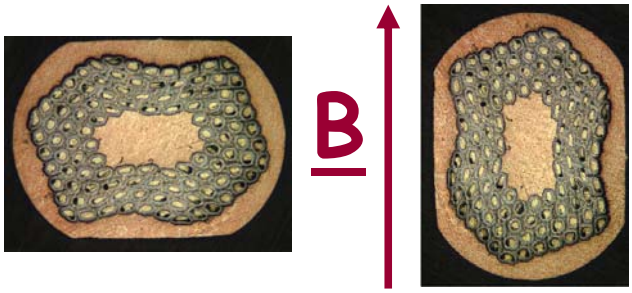

Fig. 2. Strand orientation with respect to magnetic field for I_c and I_s testing in the short edge (left) and long edge (right) configuration.

I. Sample Preparation and Test Procedures

The strand samples were wound and heat treated on grooved cylindrical barrels made of either Ti-alloy (Ti-6Al-4V) or stainless steel (SS) in Argon atmosphere. After reaction, the samples were tested on the same barrel in He at 4.2 K, in a transverse magnetic field, with relative directions of external field and transport current such as to generate an inward Lorentz force. The voltage was measured along the sample by means of voltage taps placed 50 and 75 cm apart. In the case of smooth transition from the SC to normal state, the I_c was determined from the voltage-current (VI) curve using the 10^{-14} Ω·m resistivity criterion. The I_c measurement uncertainty is typically within ±1% at 4.2 K and 12 T. At low fields, where premature quenches were observed, the transition from the SC to normal state was characterized by a quench current, I_q. Voltage-field (VH) tests were performed by ramping to a fixed transport current, and sweeping the field up and down with ramp rates of 5 to 17 mT/s in the field ranges 0-4-0 T and 4-8-4 T. If no quench was observed the current was increased and the test repeated. This test was done to determine the minimum quench current, or stability current, I_S, in the presence of a magnetic field variation.

Samples for the magnetization measurements were wound on stainless steel tubes of about 1 cm in diameter and 3 inches long. The samples were heat treated in an Argon atmosphere according to optimal schedules. After reaction the sample is slid out of the tube and slipped on a G10 holder for test using a balanced coil magnetometer. Typical cycles are between 0 and 3 T, and between 10 and 13 T, with a magnetic field ramp rate of 17 mT/s. The uncertainty on magnetization is ±1% at 1 T, less than ±4% at 12 T, and within ±6% on the effective filament diameter, d_{eff}.

Cables quench currents were measured at self-field with a SC transformer equipped with a Rogowski coil to measure the secondary current. The Nb_3Sn cable sample is part of the secondary winding. The integrated Rogowski signal (proportional to the secondary current) and the primary current from the analog output of the power supply were acquired with a NI DAQ card at 25 kHz rate.

The geometric filament sizes were obtained using a high-resolution optical microscope equipped with an imaging software that allows measuring lengths with pixel resolution, i.e. 0.72 mm. The short and long diameters were measured for all filaments on a number of cross sections with a precision of ±1 mm. The estimated accuracy was $\pm^{0}_{2.5\%}$. Due to the cables lay angle of ~14.5 degree, filament sizes measured on cable cross sections were overestimated by ~3% when parallel to the cable axis.

II. Effect of Cabling

A. Critical Current and Stability

Fig. 3 shows I_c or I_q obtained through VI and VH measurements as a function of magnetic field for the 0.7 mm 54/61 RRP strands extracted from cable 891-D. “Ti” and “SS” in legend represent Ti-6Al-4V and SS as test barrel material. These samples had been used as witnesses during reaction of mirror HFDM-04. Their RRR ranged from 7 to 33. Fig. 4 shows I_c or I_q obtained through VI and VH measurements as a function of magnetic field for 0.7 mm 54/61 RRP round strands and strands extracted from cable 911. These samples had been used as witnesses during reaction of mirror HFDM-05. The

RRR of the round strands ranged from 36 to 80, that of the extracted strands from 35 to 68. A large spread in the I_c and/ or I_s results can be observed in both cases, with an I_S scattering larger than 100% for the latter. But in a few exceptions as in Fig. 4, extracted strands typically exhibit larger instabilities than round ones [7]. Their transport current reduction is larger both in the VI and the VH tests, where their minimal quench current, I_S, is smaller than for the associated round strands. This behavior can be at least partially explained by an increase in the size of the filaments when subjected to plastic deformation during cabling, as checked and confirmed in [6] by measuring filament size distributions in cabled strands.

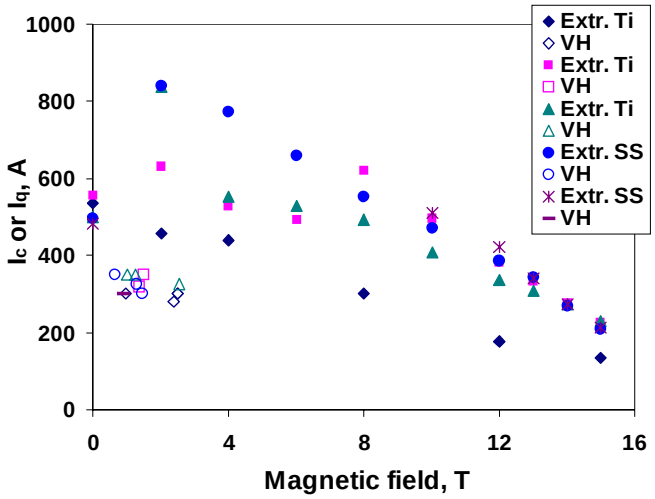

Fig. 3. I_c or I_q obtained through VI and VH measurements as a function of magnetic field for the 0.7 mm 54/61 RRP strands extracted from cable 891-D. Ti and SS in legend represent test barrel material.

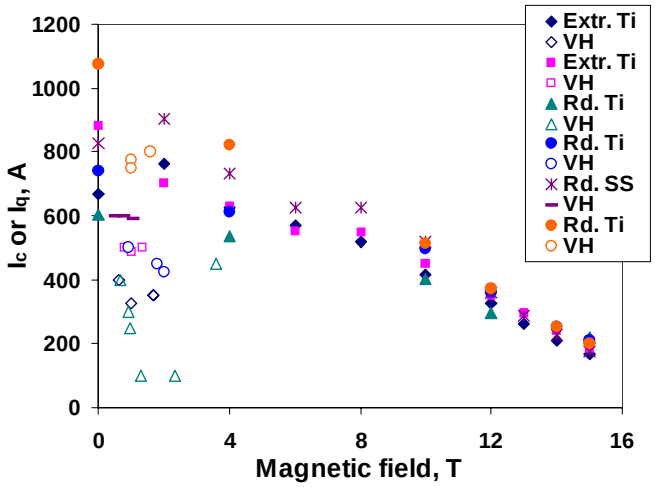

Fig. 4. I_c or I_q obtained through VI and VH measurements as a function of magnetic field for 0.7 mm 54/61 RRP round strands and strands extracted from cable 911. Ti and SS in legend represent test barrel material.

I_c and I_q results obtained through VI and VH measurements as a function of magnetic field for 1 mm 108/127 RRP round and extracted strands from cables HFDA-KS and HFDA-RC are shown in Fig. 5. The RRR of the round strands ranged from 259 to 324,

that of the extracted strands from 225 to 284. Whereas the I_S relative to the strand larger cross section has improved by more than 50% in this strand design, a scattering of ~ 80% can still be observed for I_S.

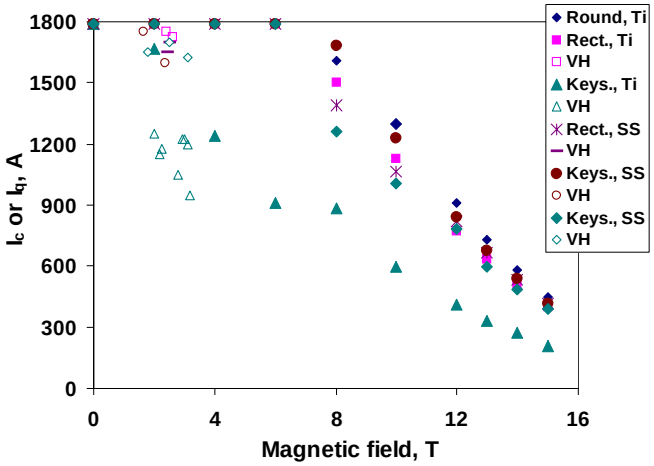

Fig. 5. I_c or I_q obtained through VI and VH measurements as a function of magnetic field for 1 mm 108/127 RRP round strands and strands extracted from cables HFDA's. Ti and SS in legend represent test barrel material.

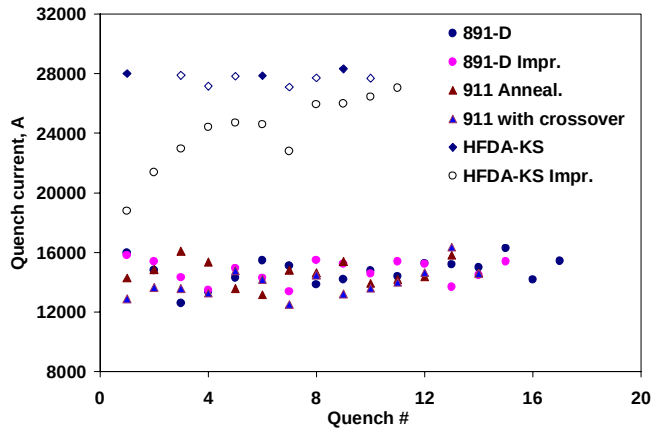

Fig. 6. Cables quench currents measured at self-field with a SC transformer. Open markers indicate the maximum current reached without any quench.

Cable samples to be measured with a SC transformer were also included as witnesses during reaction of mirrors HFDM-04 and 05. Their quench results are shown in Fig. 6. In this case with more limited statistics the spread observed was ~30% only, with quench currents per strand ranging from 320 to 420 A. A couple of samples of cable HFDA-KS were also heat treated and tested. Open markers in Figure indicate the maximum current reached without any quench. This cable appears to quench at 1030 to 1050 A per strand. Consistently with what had been observed in [5], impregnation does not have significant effect for RRP material.

B. Filament Size and Damage

To check for any increase in the size of the filaments due to cabling, several cable cross-sections were analyzed. For each deformed strand in each cross-section, the short and

long diameters were measured for all filaments. A strand is defined as deformed when its relative deformation is greater than 24.4%. Tables III and IV provide the average and maximum values of the long diameter distributions for cables 891's, 892's and HFDA's. Each column in these Tables represents a cable cross-section that was analyzed. The number of deformed strands that were counted in each cable cross-section is shown along with the number of filaments that were found broken.

TABLE III
FILAMENT SIZE AND DAMAGE IN CROSS SECTIONS OF CABLES MADE OF 54/61 RRP STRANDS

Cable ID	892-A	892-B	892-C	892-D	891-A	891-C	891-D
Cable Information	Unreacted	Unreacted	Unreacted	Unreacted	Unreacted	Unreacted	Unreacted
Ave. filament size, μm	79.7	83.0	80.8	80.5	83.7	83.2	82.0
Max. filament size, μm	106	119	104	99	109	109	112
No. Deformed Strands	5	5	3	3	2	5	20
No. Broken Filaments	1	22	0	0	0	2	11
Ave. Broken Fil./ Strand	0.2	4.4	0	0	0	0.4	0.55

TABLE IV
FILAMENT SIZE AND DAMAGE IN CROSS SECTIONS OF CABLES HFDA-RC AND HFDA-KS MADE OF 108/127 RRP STRANDS

Cable Information	Unreacted	Unreacted	Reacted	Unreacted	Unreact./Anneal.	Reacted
Cable Geometry	Rect.	Rect.	Rect.	Keys.	Keys.	Keys.
Ave. filament size, μm			75.0			75.4
Max. filament size, μm			101			101
No. Deformed Strands	5	5	4	9	14	7
No. Broken Filaments	3	0	0	0	2	0
Ave. Broken Fil./ Strand	0.6	0	0	0	0.14	0
Location Deformed Str.	1,13-15,27	1,13-15,27	1,2,13,14	1,2,10,12-16,27	1,2,6-8,14-16,22-27	1,2,14-17,27
Location Broken Fil.	14				7,15	

Relative to the average of the long diameter distribution in the unreacted 0.7 mm 54/61 RRP strand, which was 80 μm (with a maximum of 102 μm), the increase in filament size in cables 891's and 892's was always less that 5%. In the case of the reacted 1 mm 108/129 RRP strand, the average of the long diameters was 75.2 μm (with a maximum of 97 μm), which is the same as what was measured in the reacted cables HFDA's. One can see that whereas the number of deformed strands is generally larger in keystoned cables, one finds the same number or more of broken filaments per strand in rectangular cables.

For HFDA cables the locations of the deformed strands and broken filaments are also given, using the scheme in Fig. 7. It is interesting to observe that deformed strands and broken filaments were found both at the edges of rectangular and keystoned cables, but also on the straight sections in between edges. To add statistics to the analysis of the HFDA cables, cross sections of extracted strands were analyzed in the same manner, and results are shown in Table V.

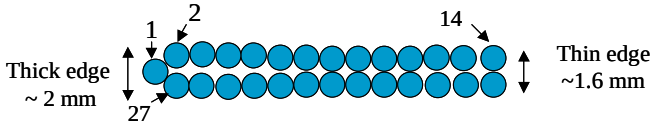

Fig. 7. Scheme of the strand locations used in Table IV for Rutherford cables.

TABLE V
FILAMENT SIZE AND DAMAGE OF 108/127 RRP STRANDS EXTRACTED FROM CABLES HFDA-RC AND HFDA-KS

Strand Information	Unreacted	Unreacted	Reacted	Reacted	Reacted
Cable Information	Extr. Rect.	Extr. Keys.	Extr. Rect.	Extr. Keys.	Extr. Keys.
Ic(12 T, 4.2 K), A	NA	NA	771	409	Q 497
No. Measured Cross-sections	2	4	2	2	2
No. Broken Filaments	8	18	5	2	6
Ave. Broken Fil./ Cross section	4	4.5	2.5	1	3

During the microscopic analysis, another phenomenon was observed. Broken filaments sometimes merged into each other, as shown for instance in Fig. 8, creating larger filaments with a somewhat continuous barrier. If filaments are fused together, the strand could see a larger d_{eff} and its instability dramatically increase. Unfortunately this could not be checked by measuring magnetization of extracted strands since the d_{eff} changes only locally in the extracted strand, and the contribution to magnetization would be negligible. To check whether there was any sintering effect of the filaments, the 1 mm 108/127 RRP round strand was rolled down to various sizes and magnetization measured for strand deformations up to 50%.

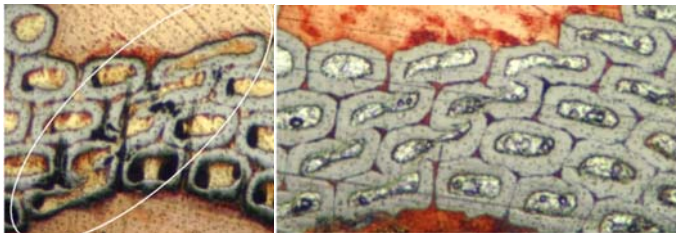

Fig. 8. Example of filament fusion in reacted (left) and unreacted (right) HFDA-RC.

III. Effect of Rolling

A. Magnetization

The rolled strands were wound on the test holder with the long edge parallel to the field, hence with the shortest size of the filaments perpendicular to the field. The magnetization curves per total volume of the 108/127 RRP round and rolled strands are shown at low field in Fig. 9. One can see that despite the decreasing rolling size, the magnetization amplitude of the 0.6 and 0.5 mm rolled strands is larger than for the round, confirming the hypothesis that at this level of deformation filament merging occurs.

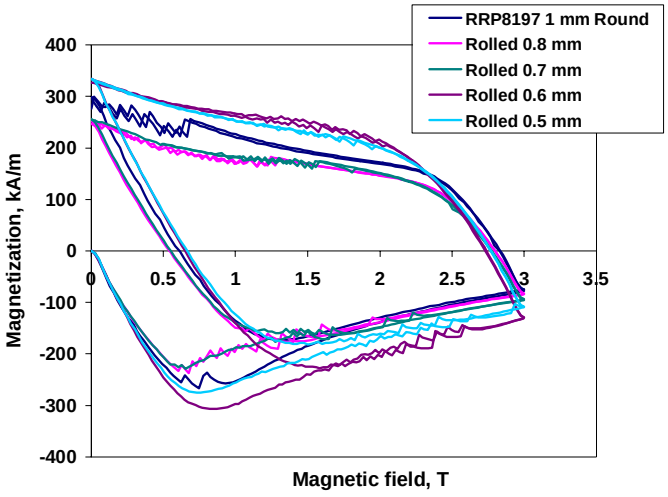

Fig. 9. Magnetization curves per total volume of 108/127 RRP round and rolled strands at low field.

B. Critical Current and Stability

The 1 mm 108/127 strand was rolled down to 0.7 mm, and the 0.7 mm 108/127 strand and 0.7 mm 90/91 strand were rolled down to 0.5 mm with the intent of testing them in both the long and short edge configurations as described in Section II. Long and short filament size distributions were measured for these rolled strands. Table VI specifies under the "$d_{geom\perp}$" row what is in each case the average size of the filaments perpendicular to the axis of the test barrel, which is parallel to the external magnetic field. The I_c at 12 T, the I_S and the RRR are given in Table. As for the extracted strands, some spread was observed in the I_c results of some of the rolled strands. "P1" under the "I_S" row denotes using a pressure contact sample holder for the test.

TABLE VI
MEASURED PROPERTIES OF ROUND AND ROLLED RRP STRANDS

Size	1 mm 8195	Rolled	Rolled	0.7 mm 8195	Rolled	Rolled	0.7 mm 8079	Rolled	Rolled
Restacks	108/127	to 0.7 mm	to 0.7 mm	108/127	to 0.5 mm	to 0.5 mm	90/91	to 0.5 mm	to 0.5 mm
Test configuration		Long edge	Short edge		Long edge	Short edge		Long edge	Short edge
Cu%	49	49	49	49	49	49	41	41	41
$d_{geom\perp}$, μm	64-75	54	88	45-54	38	62	52-65	45	78
I_c(12 T), A	880	878	778	437	428	415	500	477	Q 376
J_c(12 T), A/mm^2	2197	2192	1942	2227	2181	2114	2202	2101	Q 1656
I_s, A	1650	1750	1400	1300	850 (P1)	900	1450	775 (P1)	868
J_s, A/mm^2	4119	4369	3495	6623	4331	4586	6386	3413	3822
RRR	318	125	94	190	29	31	270	35	25

REFERENCES

[1] A.V. Zlobin et al., "Development and Test of Nb_3Sn Cos-theta Dipoles Based on PIT Strands", IEEE Trans. Appl. Sup., V. 15, No. 2, June 2005, p. 1160.

[2] S. Feher, "Development and Test of Nb_3Sn Cos-theta Magnets Based on RRP and PIT Strands", paper TUA2OR4, presented at MT-19, Genoa (Italy), September 2005.

[3] Workshop on Instabilities in Nb_3Sn Strands, Cables, and Magnets, Fermilab, April 28-30, 2004.

[4] E. Barzi et al., "Instabilities in Transport Current Measurements of Nb_3Sn Strands", IEEE Trans. Appl. Sup., V. 15, No. 2, June 2005, p. 3364.

[5] E. Barzi et al., "Study of Nb_3Sn Cable Stability at Self-field using a SC Transformer", IEEE Trans. Appl. Sup., V. 15, No. 2, June 2005, p. 1537.

[6] E. Barzi et al., "Magnetization of high-J_c Nb_3Sn Strands", TD note TD-05-051, October 14, 2005.

[7] E. Barzi et al., "Effect of temperature and deformation on Nb_3Sn Strands Instabilities", submitted to CEC/ICMC'05, Aug. 29-Sept. 2, 2005, Keystone, CO, for publication on Advances in Cryogenic Engineering.